Ultra-high resolution zone-doubled diffractive X-ray optics for the multi-keV regime

Joan Vila-Comamala,[1,*] Sergey Gorelick,[1] Elina Färm,[2] Cameron M. Kewish,[1,†] Ana Diaz,[1] Ray Barrett,[3] Vitaliy A. Guzenko,[1] Mikko Ritala,[2] and Christian David[1]

[1]*Paul Scherrer Institut, CH-5232 Villigen, Switzerland*
[2]*Department of Chemistry, University of Helsinki, FI-00014 Helsinki, Finland*
[3]*ESRF, F-38043 Grenoble Cedex 9, France*
[†]*Current address: Synchrotron SOLEIL, F-91192 Gif sur Yvette, France*
**joan.vila@psi.ch*

Abstract: X-ray microscopy based on Fresnel zone plates is a powerful technique for sub-100 nm resolution imaging of biological and inorganic materials. Here, we report on the modeling, fabrication and characterization of zone-doubled Fresnel zone plates for the multi-keV regime (4—12 keV). We demonstrate unprecedented spatial resolution by resolving 15 nm lines and spaces in scanning transmission X-ray microscopy, and focusing diffraction efficiencies of 7.5% at 6.2 keV photon energy. These developments represent a significant step towards 10 nm spatial resolution for hard X-ray energies of up to 12 keV.

OCIS codes: (110.7440) X-ray imaging; (050.1965) Diffractive lenses; (340.6720) Synchrotron radiation; (340.7440) X-ray imaging; (340.7460) X-ray microscopy.

References and links

1. M. Howells, C. Jacobsen, T. Warwick, and A. van den Bos, "Principles and applications of zone plate X-ray microscopes," in *Science of Microscopy*, Eds.: P. W. Hawkes and J. C. H. Spence (Springer New York), Chapter 13, 835–926 (2008).
2. A. Sakdinawat, and D. Attwood, "Nanoscale X-ray imaging," Nat. Photonics **4**(12), 840–848 (2010).
3. J. Kirz, C. Jacobsen, and M. Howells, "Soft X-ray microscopes and their biological applications," Q. Rev. Biophys. **28**(1), 33–130 (1995).
4. C. Jacobsen, and J. Kirz, "X-ray microscopy with synchrotron radiation," Nat. Struct. Biol. **5**(8 Suppl), 650–653 (1998).
5. H. Ade, and H. Stoll, "Near-edge X-ray absorption fine-structure microscopy of organic and magnetic materials," Nat. Mater. **8**(4), 281–290 (2009).
6. G. Schneider, "X-ray microscopy: methods and perspectives," Anal. Bioanal. Chem. **376**(5), 558–561 (2003).
7. P. Fischer, "Studying nanoscale magnetism and its dynamics with soft X-ray microscopy," IEEE Trans. Magn. **44**(7), 1900–1904 (2008).
8. J. Thieme, I. McNulty, S. Vogt, and D. Paterson, "X-ray spectromicroscopy--a tool for environmental sciences," Environ. Sci. Technol. **41**(20), 6885–6889 (2007).
9. D. Attwood, *Soft X-rays and Extreme Ultraviolet Radiation* (Cambridge University Press, 2000), Chapter 9.
10. J. Vila-Comamala, K. Jefimovs, J. Raabe, T. Pilvi, R. H. Fink, M. Senoner, A. Maassdorf, M. Ritala, and C. David, "Advanced thin film technology for ultrahigh resolution X-ray microscopy," Ultramicroscopy **109**(11), 1360–1364 (2009).
11. W. Chao, J. Kim, S. Rekawa, P. Fischer, and E. H. Anderson, "Demonstration of 12 nm resolution Fresnel zone plate lens based soft x-ray microscopy," Opt. Express **17**(20), 17669–17677 (2009).
12. S. Rehbein, S. Heim, P. Guttmann, S. Werner, and G. Schneider, "Ultrahigh-resolution soft-x-ray microscopy with zone plates in high orders of diffraction," Phys. Rev. Lett. **103**(11), 110801 (2009).
13. C. Jacobsen, "Soft x-ray microscopy," Trends Cell Biol. **9**(2), 44–47 (1999).
14. Y. Feng, M. Feser, A. Lyon, S. Rishton, X. Zeng, S. Chen, S. Sassolini, and W. Yun, "Nanofabrication of high aspect ratio 24 nm X-ray zone plates for X-ray imaging applications," J. Vac. Sci. Technol. B **25**(6), 2004 (2007).
15. Y. T. Chen, T. N. Lo, C. W. Chiu, J. Y. Wang, C. L. Wang, C. J. Liu, S. R. Wu, S. T. Jeng, C. C. Yang, J. Shiue, C. H. Chen, Y. Hwu, G. C. Yin, H. M. Lin, J. H. Je, and G. Margaritondo, "Fabrication of high-aspect-ratio Fresnel zone plates by e-beam lithography and electroplating," J. Synchrotron Radiat. **15**(2), 170–175 (2008).
16. J. Vila-Comamala, M. Dierolf, C. M. Kewish, P. Thibault, T. Pilvi, E. Färm, V. Guzenko, S. Gorelick, A. Menzel, O. Bunk, M. Ritala, F. Pfeiffer, C. David, M. Denecke, and C. T. Walker, "High spatial resolution STXM at 6.2 keV photon energy," AIP Conf. Proc. **1221**, 80–84 (2010).
17. K. Jefimovs, J. Vila-Comamala, T. Pilvi, J. Raabe, M. Ritala, and C. David, "Zone-doubling technique to produce ultrahigh-resolution x-ray optics," Phys. Rev. Lett. **99**(26), 264801 (2007).

#136632 - $15.00 USD Received 21 Oct 2010; revised 10 Dec 2010; accepted 17 Dec 2010; published 22 Dec 2010

18. D. C. Flanders, and N. N. Efremow, "Generation of < 50 nm period gratings using edge defined techniques," J. Vac. Sci. Technol. B **1**(4), 1105–1108 (1983).
19. Y.-K. Choi, T.-J. King, and C. Hu, "A spacer patterning technology for nanoscale CMOS," IEEE Trans. Electron. Dev. **49**(3), 436–441 (2002).
20. P. Charalambous, and A. Firsova, "Enhancement of zone plate efficiency by evaporation" in *X-ray Microscopy IV (Proc. of the 4th Intern. Conf.)*, Eds.: V. V. Aristov and A. I. Erko (Chernogolovka, Russia) 504–509 (1994).
21. T. Aaltonen, M. Ritala, V. Sammelselg, and M. Leskela, "Atomic layer deposition of iridium thin films," J. Electrochem. Soc. **151**(8), G489–G492 (2004).
22. J. W. Goodman, *Introduction to Fourier optics* (McGraw-Hill International Editions, 1996), Chapter 2.
23. J. A. Ferrari, "Fast Hankel transform of order zero," J. Opt. Soc. Am. A **12**(8), 1812–1813 (1995).
24. J. A. Ferrari, D. Perciante, and A. Dubra, "Fast Hankel transform of nth order," J. Opt. Soc. Am. A **16**(10), 2581–2582 (1999).
25. M. Born, and E. Wolf, *Principles of optics, 7th (expanded) Edition* (Cambridge University Press, 1999), Chaper 8.
26. J. Vila-Comamala, S. Gorelick, V. A. Guzenko, E. Färm, M. Ritala, and C. David, "Dense high aspect ratio hydrogen silsesquioxane nanostructures by 100 keV electron beam lithography," Nanotechnology **21**(28), 285305 (2010).
27. DECTRIS Ltd, Neuenhoferstrasse 107, CH-5400 Baden, Switzerland. URL: *http://www.dectris.ch*
28. B. Hornberger, M. Feser, and C. Jacobsen, "Quantitative amplitude and phase contrast imaging in a scanning transmission X-ray microscope," Ultramicroscopy **107**(8), 644–655 (2007).
29. M. D. de Jonge, B. Hornberger, C. Holzner, D. Legnini, D. Paterson, I. McNulty, C. Jacobsen, and S. Vogt, "Quantitative phase imaging with a scanning transmission x-ray microscope," Phys. Rev. Lett. **100**(16), 163902 (2008).
30. A. Menzel, C. M. Kewish, P. Kraft, B. Henrich, K. Jefimovs, J. Vila-Comamala, C. David, M. Dierolf, P. Thibault, F. Pfeiffer, and O. Bunk, "Scanning transmission X-ray microscopy with a fast framing pixel detector," Ultramicroscopy **110**(9), 1143–1147 (2010).

1. Introduction

X-ray imaging, in particular X-ray microscopy [1,2], is an appealing technique for the inspection of both organic [3–5] and inorganic [6–8] materials. Its prospects rely on a combination of high spatial resolution, high penetrating power, analytical chemical sensitivity and compatibility with wet specimens, without the cumbersome sample preparation required by other imaging techniques such as transmission electron microscopy.

Fresnel zone plates (FZPs) [9] are widely used diffractive optical elements for X-ray focusing and imaging. Progress on the fabrication of these optical devices plays a key role in improving the performance of FZP-based X-ray microscopes; for instance, their spatial resolution is limited to the width of outermost zone of the FZP, Δr. To date, electron-beam lithography (EBL) has been the most successful technique for producing diffractive X-ray optics since this approach is capable of writing patterns with a precision and an electron beam spot size of a few nanometers. The smallest features that can be reliably manufactured are, however, limited by the electron scattering in the exposed resist material. This effect is particularly detrimental when writing dense patterns and has become a fundamental limit in the manufacturing of diffractive X-ray optics. Due to this limitation, soft X-ray (0.2—2 keV) microscopes typically operate with minimum spatial resolutions of 30 to 25 nm, and sub-20 nm features have only been resolved in a few cases [10–12]. Although many specimens can be investigated at this low energy range [13], higher X-ray energies provide access to a broader range of chemical specificities and allow for the investigation of significantly thicker samples due to the higher penetration depth of the radiation. Nevertheless, the fabrication of FZPs for hard X-ray photon energies is more challenging because the dense lens pattern must be transferred into extremely high aspect ratio (*e.g.*, > 20) structures to provide satisfactory diffraction efficiency. In the multi-keV regime (4—12 keV), FZPs have delivered spot sizes below 50 nm [14–16] but sub-25 nm spatial resolution has not been yet reported.

To surpass the intrinsic limitations that EBL imposes on the manufacture of diffractive X-ray optics, we introduced a zone-doubling approach [17] that overcomes the difficulty of high feature density patterning and allows us to produce extremely high aspect ratio structures with lateral dimensions in the sub-50 nm regime. This technique resembles the so-called iterated spacer lithography [18–20] and is based on the deposition of a thin layer of high refractive index material onto the sidewalls of a pre-patterned template made of a low refractive index material. This leads to an effective line density doubling in the deposited material compared to

#136632 - $15.00 USD Received 21 Oct 2010; revised 10 Dec 2010; accepted 17 Dec 2010; published 22 Dec 2010

that of the template. Here, we report on the modeling, fabrication and characterization of zone-doubled FZPs for the multi-keV regime. Using wavefront calculations, we compare the behavior and performance of ordinary and zone-doubled FZPs in simulated experiments. We derive relevant information such as the position, shape and efficiency of the foci corresponding to any diffraction order. Subsequently, we report on the fabrication of the zone-doubled FZPs and their characterization as focusing elements in scanning transmission X-ray microscopy.

2. Zone-doubled Fresnel zone plate design and modeling

Zone-doubled diffractive X-ray optics are made of a combination of two materials with low and high refractive indices. For X-ray energies, the refractive index of a material, n, is represented by the complex expression $n = 1 - \delta + i\beta$. The real coefficient δ denotes the phase shifting component, while the β coefficient of the imaginary part accounts for the X-ray absorption in the material. Higher values of δ and β imply a stronger interaction between the X-rays and the material. Here, materials with high refractive indices must be understood as materials with high values of δ and β. As previously reported [10,17], this manufacturing approach exploits the fact that the patterning of sparse structures by EBL is advantageous, and the possibility to metal-coat a surface uniformly and conformally by atomic layer deposition (ALD) [21]. Figure 1 shows a drawing of a zone-doubled FZP made of hydrogen silsesquioxane (HSQ) resist and iridium. HSQ is a negative tone EBL resist transforming into a SiO_2-like material after irradiation by electrons, photons or ions and development in a buffered alkaline solution. The iridium line density at the outer regions of the structure is effectively doubled in comparison to that of the HSQ resist template. The effective outermost zone width, Δr, of the zone-doubled element coincides with the thickness, w, of the uniform layer of iridium coating the template.

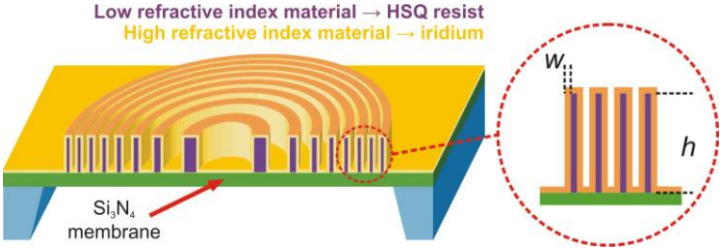

Fig. 1. Schematic illustration of a zone-doubled FZP made of HSQ resist and iridium. The HSQ resist template is coated by a uniform layer of iridium of thickness w, which matches the outermost zone width of the FZP, Δr. The structures have an iridium zone height h.

The geometry of a zone-doubled FZP is significantly different from that of a conventional FZP. Diffraction efficiency calculations of zone-doubled FZPs were already assessed in [17] but further insight can be gained by comparing the propagation of a planar illuminating X-ray wavefront after interaction with both ordinary and zone-doubled FZPs. Here, we have implemented the Fresnel propagation of a circularly symmetric wavefront by means of the zeroth-order Hankel transform of a one dimensional radial refractive index profile [22]. To our knowledge, the amount of input points accepted by standard Hankel transform computation routines is normally limited to a few thousand, due to extremely high and unattainable computer memory requirements. However, a much larger number of points is required to accurately model X-ray FZP refractive index profiles which can be as wide as a few hundreds of microns in diameter and comprised of rings that can be as small as 10 nm. To achieve a precision of 0.5 nm for a 100 µm diameter FZP, we required the zeroth-order Hankel transform of a profile containing $N = 10^5$ points. A MATLAB code was implemented following the method of Ferrari *et al.* [23,24]. The simulated wavefront is then sampled with an accuracy of 0.5 nm and the intensity distribution created by a large 100 µm diameter FZP is well-reproduced.

#136632 - $15.00 USD Received 21 Oct 2010; revised 10 Dec 2010; accepted 17 Dec 2010; published 22 Dec 2010

Figure 2 shows the results of the Fresnel wavefront propagation for a photon energy of 6.2 keV (corresponding to hard X-rays of wavelength, λ, of 0.2 nm). The calculations assumed a FZP diameter of 100 μm, a central stop diameter of 35 μm and an iridium zone height, h, of 600 nm. The central stop consists of a thick, absorbing circular obstruction that is aligned at the center of the FZP. It stops the propagation of the zeroth-order radiation and in combination with an order sorting aperture removes the unwanted diffraction orders to create a clean focus. The FZPs were modeled as a complex transmission function described by the zone-plate equation and the refractive index of the component materials. Diffraction and refraction effects within the FZP volume were neglected, that is, we assume the kinematic diffraction approximation of a "thin" zone plate that holds in grating structures as long as the period-to-wavelength ratio is high and as long as the element is not too thick. Figure 2(a) shows the calculated intensity distribution along the optical axis behind an ordinary FZP made of iridium, and an outermost zone width of $\Delta r = 40$ nm. The wavefront is propagated from the optical element located at 0 mm to its 1st order focal spot located at a distance $f_1 = 20$ mm from the exit pupil. Several foci corresponding to the odd diffraction orders can be identified. In comparison with this conventional FZP, Fig. 2(b) shows the intensity distribution calculated for a zone-doubled FZP made of HSQ resist and iridium with an effective outermost zone width of $w = \Delta r = 20$ nm. The zone-doubled structure has a main focal spot corresponding to its 1st diffraction order located at a distance $f_1 = 10$ mm. We note that a conventional FZP with $\Delta r = 40$ nm and a zone-doubled FZP with $w = \Delta r = 20$ nm were compared because both elements have to be written with similar line periodicity during the EBL step. As a consequence of the doubling, the main 1st diffraction order focus of the zone-doubled structure is shifted from 20 to 10 mm and the focal spot size is also expected to shrink by a factor of two. The zone-doubled FZP concentrates some intensity at a distance of 20 mm, creating a faint focal spot that originates from the periodicity of the HSQ resist template that has half of the spatial frequency of the iridium structures; it can be interpreted as a sub-harmonic order of the structure. In addition, the zone-doubled lenses have a significant 2nd order focus that is not expected for a conventional FZP. This extra focal spot arises because the uniform coating over the whole HSQ resist template leads to a departure from the ideal 1:1 line-to-space ratio for most of the zones in the FZP pattern. Figure 2(c) represents a refined intensity calculation in the vicinity of the 1st diffraction order focus of the zone-doubled FZP, from which one can estimate a depth of focus of $DOF = 8.0$ μm that matches the analytically derived value, $DOF = (\Delta r)^2/\lambda$.

Figure 2(d) shows the focal spot intensity profiles under different conditions, allowing us to assess the effect of the zone-doubling on the shape of the focal spot. All intensity profiles in the figure have been normalized to their peak values for ease of comparison. The intensity profile for the 1st order focus of an ordinary iridium FZP with $\Delta r = 20$ nm matches the analytically expected Airy pattern. The insertion of a central stop has the expected effect of slightly narrowing the central peak and somewhat increasing the intensity of the side lobes of the profile [25]. The curves corresponding to the shapes of the focal spots for the 1st and 2nd diffraction orders of a zone-doubled FZP with $w = \Delta r = 20$ nm made of HSQ resist and iridium from Fig. 2(b) are also shown. The intensity profile of the 1st order focus is not substantially different from that of an ordinary FZP, that is, the zone-doubling process does not have any significant impact on the shape of the focal spot.

#136632 - $15.00 USD Received 21 Oct 2010; revised 10 Dec 2010; accepted 17 Dec 2010; published 22 Dec 2010

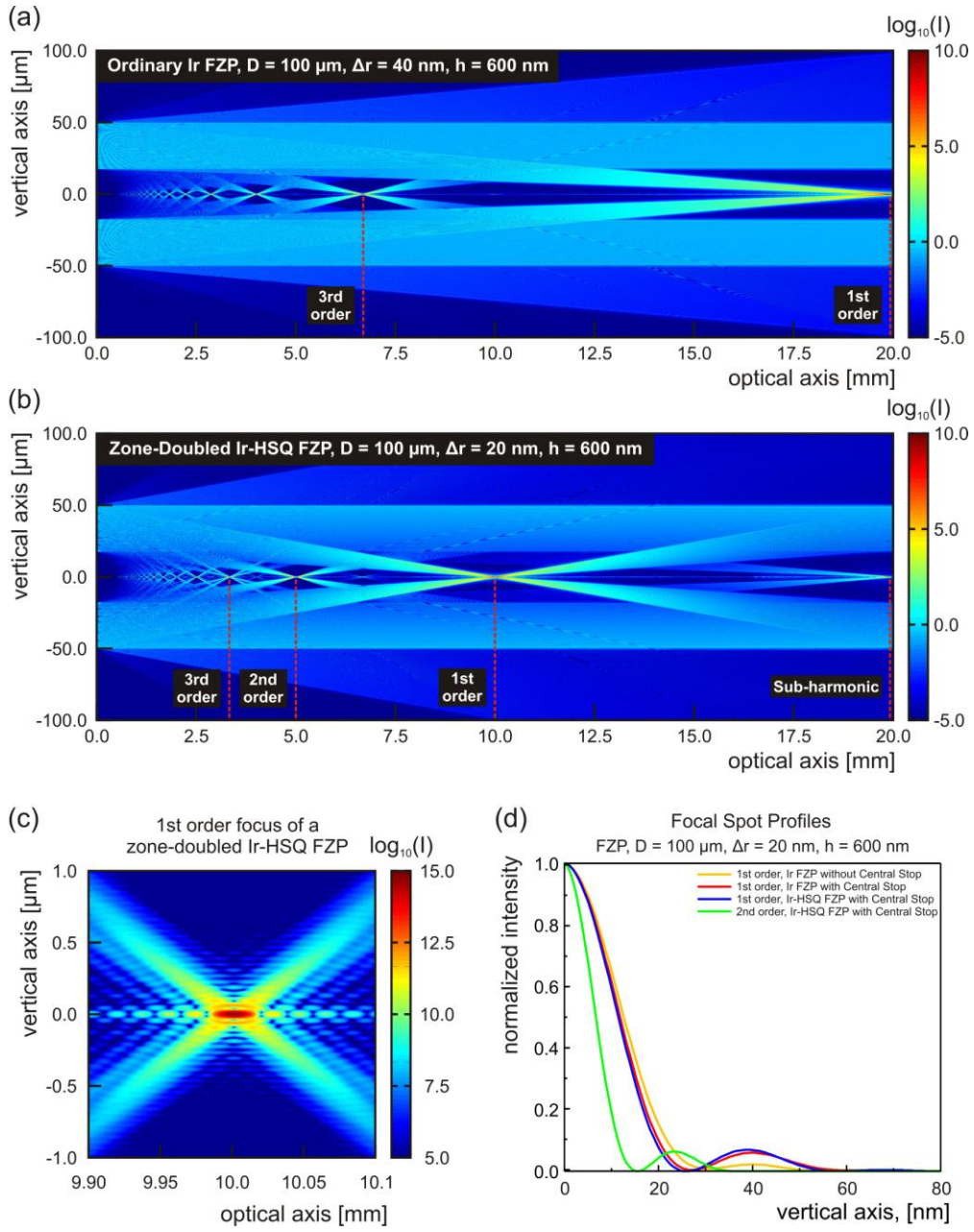

Fig. 2. Comparison of the Fresnel wavefront propagation for (a) an ordinary FZP with an outermost zone width of Δr = 40 nm and (b) a zone-doubled FZP with an effective outermost zone width of $w = \Delta r$ = 20 nm. For both structures, a similar line periodicity has to be written during the electron beam lithography step. In the calculations, the lens diameter was 100 µm, the iridium zone height, h, was 600 nm, the central stop diameter was 35 µm and the photon energy was 6.2 keV. The positions of the foci corresponding to several diffraction orders are indicated. (c) Beam waist in the vicinity of the 1st order focus of the zone-doubled FZP, showing a depth of focus, *DOF*, of 8 µm. (d) Comparison of the calculated intensity profiles at the focus under several conditions. All intensities were normalized to peak values for ease of comparison. There is no significant shape difference between the focal spots of ordinary and zone-doubled FZPs. A 2nd order focus with a spot size reduced by a factor of two in comparison to the 1st order focus is expected for the zone-doubled diffractive lenses.

#136632 - $15.00 USD Received 21 Oct 2010; revised 10 Dec 2010; accepted 17 Dec 2010; published 22 Dec 2010

The diffraction efficiency, that is, the fraction of the incoming intensity delivered into a particular diffraction order, can also be calculated from the intensity distributions in Fig. 2. Table 1 summarizes the calculated diffraction efficiencies for the most relevant diffraction orders of the ordinary and the zone-doubled FZPs for a photon energy of 6.2 keV from Figs. 2(a) and (b). Despite the X-ray absorption in the HSQ resist template and the uniform iridium coating over the whole FZP pattern, a 600 nm-tall zone-doubled structure is calculated to have 13% diffraction efficiency for the 1st order focus. This is an acceptable decrease relative to the 18% diffraction efficiency that could be obtained for a conventional FZP providing only half of the resolving power. In addition, 2% efficiency is expected for the 2nd order focus of the zone-doubled FZP. Since the focal spot size corresponding to this 2nd diffraction order is a factor of two smaller than the 1st order focus, it could potentially be used to achieve higher spatial resolution imaging and will be investigated in future work. The residual sub-harmonic focus originated by the HSQ template in the zone-doubled FZP has a very low diffraction efficiency of 0.35%.

Table 1. Calculated diffraction efficiencies for ordinary and zone-doubled FZPs at 6.2 keV photon energy from the wavefront propagation in Fig. 2. The structures are made of an iridium height of h = 600 nm.

	diffraction order	DE[%]
Ordinary Ir FZP, Δr = 40 nm	1st	18.40
	3rd	2.08
Zone-doubled Ir-HSQ FZP $w = \Delta r$ = 20 nm	Sub-harmonic (½th)	0.35
	1st	13.10
	2nd	2.00
	3rd	0.97

3. Zone-doubled Fresnel zone plate fabrication

The production of the zone-doubled FZPs starts using 100 keV EBL to expose template patterns onto a 550—600 nm-thick layer of HSQ resist spin-coated on 200 nm-thick silicon nitride (Si_3N_4) membranes. The exposures were performed with a Vistec EBPG5000Plus EBL tool. The HSQ resist was developed with a high contrast developer (buffered sodium hydroxide solution) followed by supercritical drying in carbon dioxide. Subsequently, the HSQ templates were iridium coated by ALD [21]. Further and extensive details of the manufacturing process can be found in [26] and the references therein.

Figure 3 shows several scanning electron micrographs of a zone-doubled FZP made of HSQ resist and iridium. The lens diameter is 100 µm and its effective outermost zone width is $w = \Delta r$ = 20 nm. Low magnification images in Figs. 3(a) and (b) show overviews of the HSQ template prior to the iridium coating by ALD and illustrates the capability of patterning large defect-free elements. Figures 3(c) shows a high magnification top view of 20 nm-wide lines made of HSQ resist with 80 nm period at the outermost part of the HSQ template. Figure 3(d) shows an equivalent region after the iridium coating demonstrating the high accuracy of the deposition. In regions of the template containing structures below 150 nm in width, the zones were buttressed by narrow connecting spokes to prevent their collapse as a result of surface tension forces of the liquid trapped in the pattern during development. The buttressing density was gradually increased as a function of the FZP radius. Finally, Figs. 3(e) and 3(f) show tilted views of the edge of the zone-doubled FZP before and after iridium deposition, acquired at a tilt angle of 50°. The measured height, h, of the zones is ~ 550 nm and therefore, the zone-doubled FZP is made of an effective iridium grating of 20 nm-wide structures having an aspect ratio of h/w = 27.5. The scanning electron micrographs demonstrate the quality of the EBL and there are only occasional defects created during the processing of chips that might jeopardize the performance of some of the FZPs.

We have used this approach to manufacture zone-doubled FZPs for the multi-keV regime with diameters up to 150 µm and outermost zone widths between 30 and 15 nm. Our fabrication method has proven to be robust and reliable, in terms of reproducibility and high fabrication yield.

#136632 - $15.00 USD Received 21 Oct 2010; revised 10 Dec 2010; accepted 17 Dec 2010; published 22 Dec 2010

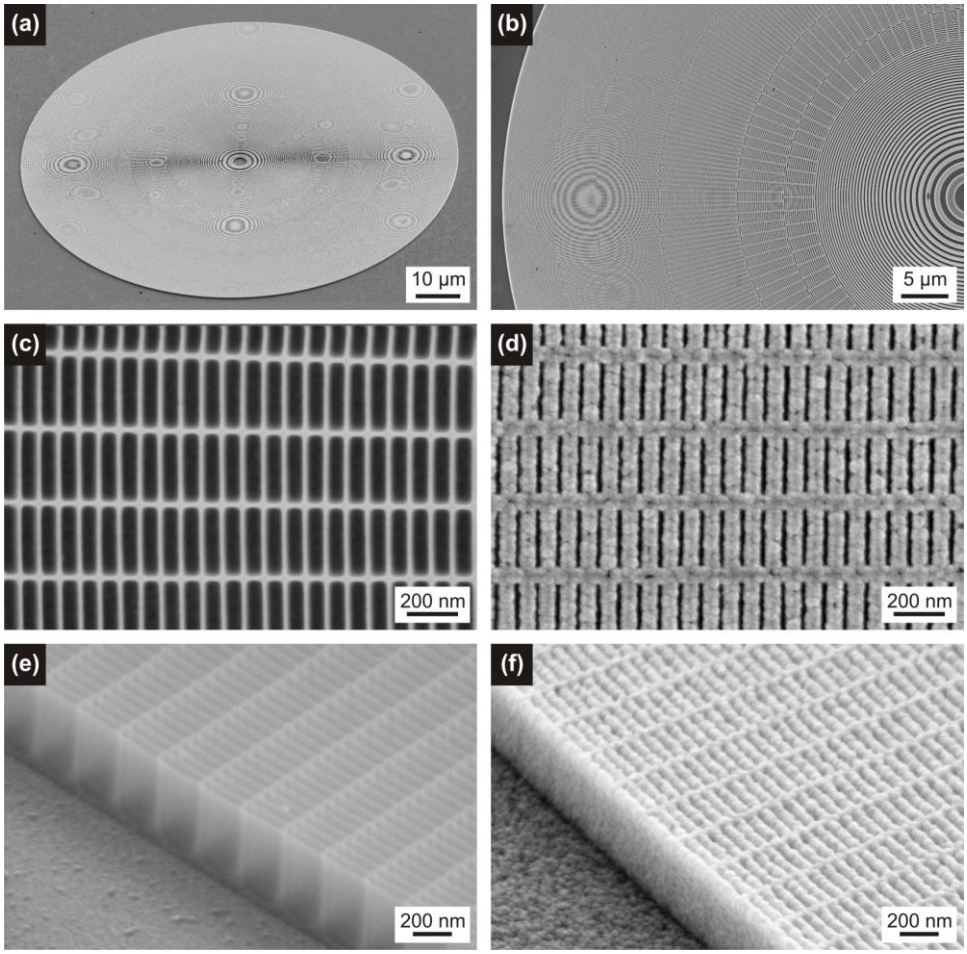

Fig. 3. Scanning electron micrographs of a zone-doubled FZP made of HSQ resist and iridium (100 µm diameter, outermost zone width of $w = \Delta r = 20$ nm and height of h ~550 nm). (a) and (b) show overviews of the diffractive X-ray lens. (c) High magnification top view of the outermost region consisting of 20 nm-wide lines made of HSQ resist in 80 nm period before the iridium coating. (d) High magnification top view of the zone-doubled structure after the iridium coating by atomic layer deposition. Tilted views (at 50°) of the edge of the zone-doubled FZP (e) before and (f) after the iridium deposition. The final structure contains an effective iridium grating made of 20 nm lines and spaces with an aspect ratio of $h/w > 27.5$.

4. Zone-doubled Fresnel zone plate characterization

The zone-doubled FZPs were characterized as focusing devices at the optical test bench of ID06 beamline of the European Synchrotron Radiation Facility (ESRF) and at the coherent small-angle X-ray scattering beamline, cSAXS, of the Swiss Light Source (SLS).

The scanning transmission X-ray microscopy (STXM) setup consisted of a zone-doubled FZP, a central stop to obstruct the zeroth-order (*i.e.*, transmitted) radiation and an order-sorting aperture used to select the 1st order diffraction cone. The sample, mounted on a piezoelectric positioning stage for high-resolution scanning, was located at the 1st order focal plane. An X-ray detector located behind the sample collected the intensity transmitted and refracted by the sample.

During the experiments at the ID06 beamline (ESRF), a 100 µm diameter zone-doubled FZP was positioned at 57 m from an undulator insertion device giving a source size of 980 × 25 µm^2 (H × V). The X-ray beam illuminating the FZP had an expected transverse coherence length (FWHM) of about 10 × 250 µm^2 (H × V). Under these conditions, it was not possible

#136632 - $15.00 USD Received 21 Oct 2010; revised 10 Dec 2010; accepted 17 Dec 2010; published 22 Dec 2010

to coherently illuminate the full FZP in the horizontal direction. Consequently, the focal spot was expected to be diffraction-limited only along the vertical direction. Photons of energy 6.2 keV were selected from the undulator beam by a double-crystal monochromator and a photodiode located a few centimeters after the sample was used to record the transmitted intensity. The zone-doubled FZP had an outermost zone width of $w = \Delta r = 20$ nm and an iridium zone height of h ~550 nm. As a high resolution test sample we used another zone-doubled structure containing an iridium grating made of 20 nm lines and spaces. Figure 4(a) shows the transmission profile from a line scan along the vertical direction over an area of the iridium grating. The modulation of the measured signal clearly shows well-resolved 20 nm lines and spaces and one can distinguish between the features in the structure: the gaps, the iridium lines and the HSQ resist template. The STXM scan was acquired using a dwell time of 50 ms and a step size of 5 nm.

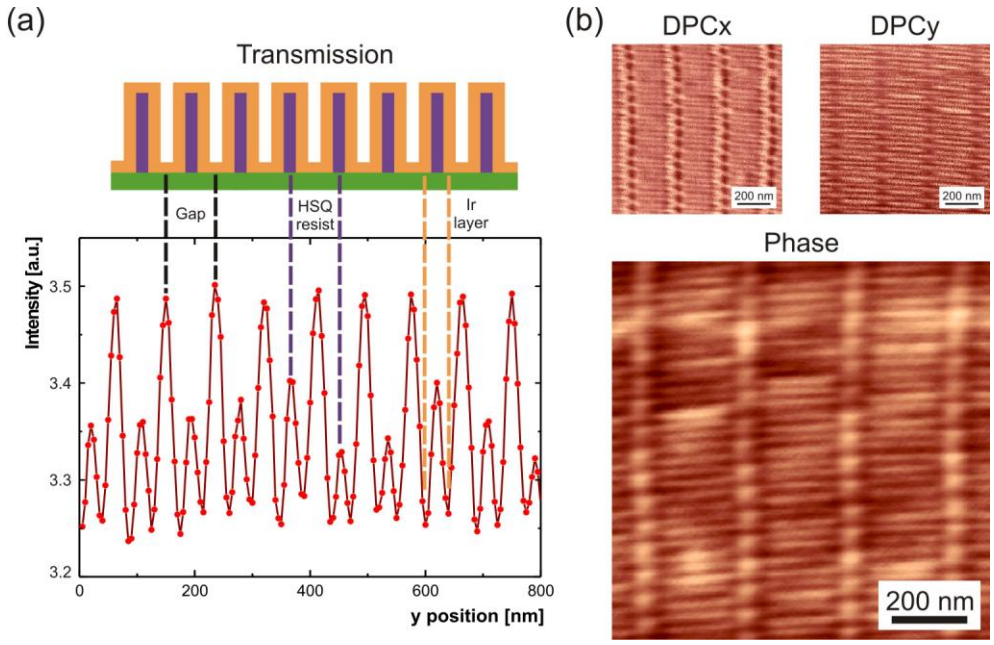

Fig. 4. STXM images acquired using zone-doubled FZPs with a diameter of 100 µm. (a) Transmission signal from zone-doubled grating containing 20 nm lines and spaces. The gaps, the iridium lines and HSQ resist template can be clearly distinguished. The scan was acquired using a FZP with an outermost zone width of $w = \Delta r = 20$ nm, a dwell time of 50 ms and step size of 5 nm (ID06 beamline, ESRF). (b) Differential phase contrast (DPCx and DPCy) and phase images from a zone-doubled grating made of 15 nm lines and spaces. The differential phase contrast images were calculated from the displacement of the full divergent radiation cone recorded by the PILATUS 2M pixel detector at each scanning position. The phase was obtained by integration from the differential phase contrast images. The image was acquired using a FZP with an outermost zone width of $w = \Delta r = 15$ nm, a dwell time of 15 ms and a step size of 2.5 nm (cSAXS beamline, SLS).

During the experiments at cSAXS beamline, the X-ray radiation was produced by an undulator insertion device with a source size estimated to be about 200 × 20 µm^2 (H × V). The monochromatic beam was vertically pre-focused using the beamline optics, to double its intensity. The transverse coherence length (FWHM) at the position of the FZP, at roughly 34.5 m from the source, was therefore expected to be 25 × 200 µm^2 (H × V) at 6.2 keV photon energy. The zone-doubled FZP used to focus the incoming X-ray beam had a diameter of 100 µm, an outermost zone width of $w = \Delta r = 15$ nm and an iridium zone height of h ~ 350 nm. The detector was positioned 7 m downstream of the focal plane, behind a He-filled flight tube to avoid excessive absorption and scattering by air. The spatially resolving PILATUS 2M pixel detector [27], operated in single photon counting mode, was used to record the full

#136632 - $15.00 USD Received 21 Oct 2010; revised 10 Dec 2010; accepted 17 Dec 2010; published 22 Dec 2010

divergent radiation cone emanating from the sample. For every scan, the variations in intensity and position of the cone footprint on the active area of the detector were processed to derive absorption, differential phase contrast (DPC) and dark field images of the sample [28–30]. A phase contrast image of the sample was also obtained by integration of the DPC images. This analysis is especially beneficial for specimens that are weakly interacting with the X-ray beam and have low contrast in transmission. A zone-doubled iridium grating containing 15 nm lines and spaces was used as a high-resolution test sample. Figure 4(b) displays the DPC images of the grating, and the phase signal obtained by integration. An area of 1x1 μm^2 of the structure was scanned using a step size of 2.5 nm and a dwell time of 15 ms. The 15 nm lines and spaces were resolved and demonstrate an unprecedented resolution in STXM for the multi-keV photon energies.

The spatial resolution tests were complemented by measurements of the focusing diffraction efficiency (ID06 beamline, ESRF). We measured the intensity concentrated into the 1st order focus of several zone-doubled FZPs with a 100 µm diameter and outermost zone widths of 30, 25, 20 and 15 nm. To obtain the diffraction efficiency of a FZP, two different intensity measurements were done: (1) the intensity of the 1st order was obtained by scanning a 5 µm diameter pinhole along the both vertical and horizontal directions at the focal plane, measuring the signal of the central plateau and subtracting the background signal, mostly originated by the zeroth-order of the lens. The transmitted background through a 5 µm diameter aperture is sufficiently small and smaller apertures are not commercially available; (2) the incoming intensity was measured by removing the FZP and placing a 100 µm aperture at the same position. Then, the diffraction intensity was obtained as the ratio of the two measured intensities. The initial measurements were done at a photon energy of 6.2 keV. Table 2 compares the experimental and calculated diffraction efficiencies for several zone-doubled FZPs. A maximum value of 7.55% diffraction efficiency was measured for a FZP with an outermost zone width of 25 nm. On average, the measured values are about 45-60% of the simulated diffraction efficiencies.. The difference can be attributed partly to absorption in the buttressing, which was not included during the calculations, and partly to the existence of defects in the fabricated zone-doubled FZPs.

Table 2. Calculated and measured 1st order diffraction efficiencies of 100 µm diameter zone-doubled FZPs at 6.2 keV photon energy.

Δr [nm]	*h* [nm]	Calculated DE [%]	Measured DE [%]
30	~550	11.10	6.05
25	~550	11.60	7.55
20	~550	12.15	4.97
15	~350	5.70	1.15

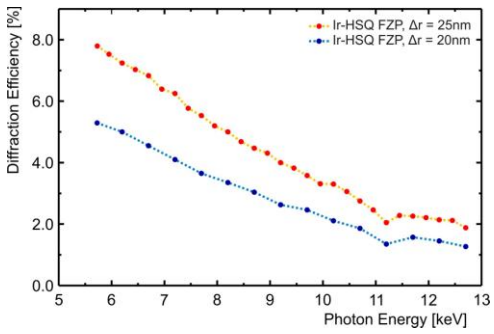

Fig. 5. Experimentally obtained 1st order diffraction efficiency of zone-doubled FZPs as function of photon energy. The structures have a 100 µm diameter, an iridium zone height of *h* ~550 nm and outermost zone widths, $w = \Delta r$, of 25 and 20 nm.

#136632 - $15.00 USD Received 21 Oct 2010; revised 10 Dec 2010; accepted 17 Dec 2010; published 22 Dec 2010

For two zone-doubled FZPs the diffraction efficiency was obtained as a function of photon energy from 5.7 to 12.7 keV. Figure 5 shows the results for zone-doubled FZPs with 25 and 20 nm outermost zone widths. As expected the diffraction efficiency decreases at higher energies dropping to about 3% at 10.0 keV. The effect of the iridium absorption edge causing a reduction in the efficiency is perceptible at 11.2 keV.

To date, the zone-doubled Fresnel zone plates have only been kept continuously in hard X-ray beams for short periods of time, up to a couple of weeks, for which no degradation of the performance has been observed. Thus, it is not yet possible to estimate the lifetime of these new diffractive optics. Nevertheless, the HSQ template is essentially SiO_2, and should be radiation hard.

5. Conclusions

We have demonstrated the feasibility of using zone-doubled diffractive X-ray optics for high resolution imaging in the multi-keV regime (4—12 keV). The zone-doubling technique was successfully employed to bypass the limitations of electron beam lithography for the patterning of dense nanostructures and provides us with a method to fabricate Fresnel zone plates with smaller outermost zone widths and higher aspect ratios than previously attainable. Wave-optical calculations demonstrated that the zone-doubling process did not have any significant effect on the shape of the focal spot created by this modified type of diffractive lenses when compared to conventional Fresnel zone plates. By using state-of-the-art nanofabrication techniques, we have produced zone-doubled Fresnel zone plates with outermost zone widths down to 20 and 15 nm and aspect ratios higher than 25. We used these lenses to achieve unprecedented spatial resolution by resolving 15 nm lines and spaces in scanning transmission X-ray micrographs. We have also measured a diffraction efficiency of 7.5% at 6.2 keV photon energy for a zone-doubled Fresnel zone plate with an outermost zone width of $w = \Delta r = 25$ nm. Due to its robustness and reliability, the zone-doubling technique offers significant advantages in terms of reproducibility and the high fabrication yield. This manufacturing approach can provide Fresnel zone plates to routinely achieve sub-25 nm spatial resolution for X-ray microscopes operating in the multi-keV regime. These developments represent a significant step towards 10 nm spatial resolution for hard X-ray photon energies up to 12 keV.

Acknowledgements

The authors are grateful to M. Bednarzik, B. Haas, A.Weber, E. Deckardt and A. Lücke for their assistance during substrate preparation. The authors would like to thank O. Bunk and A. Menzel for their assistance at the cSAXS beamline of the Swiss Light Source and C. Detlefs and T. Roth for their assistance at the ID06 beamline of the European Synchrotron Radiation Facility. The research leading to these results has received funding from the European Community's Seventh Framework Programme (FP7/2007-2013) under grant agreement No. 226716 and from the Collaborative Project NFFA-Nanoscale Foundries and Fine Analysis under grant agreement No. 212348. The synchrotron radiation measurements were performed at the Swiss Light Source, Paul Scherrer Institut (Villigen, Switzerland) and at the European Synchrotron Radiation Facility (Grenoble, France).

#136632 - $15.00 USD Received 21 Oct 2010; revised 10 Dec 2010; accepted 17 Dec 2010; published 22 Dec 2010